water

MDPI

Article

Study on Shallow Landslide Induced by Extreme Rainfall: A Case Study of Qichun County, Hubei, China

Yousheng Li, Echuan Yan * and Weibo Xiao

Faculty of Engineering, China University of Geosciences, Wuhan 430074, China; liys7589629@163.com (Y.L.)
* Correspondence: yecyec6970@163.com

Abstract: In light of the increasing frequency of extreme rainfall events, there has been a concomitant rise in landslides triggered by such precipitation. Despite the extensive research conducted on rainfall-induced landslides, the practical implementation of these findings is constrained by geological and environmental factors. Notably, there is a paucity of research on rainfall-induced shallow landslides in Hubei Province, China. Therefore, this study analyzes the fundamental characteristics and rainfall characteristics of landslides induced by multiple rounds of extreme rainfall in Qichun County in June and July 2016. The study explores the influence of five variables—namely, altitude, slope, slope aspect, stratum lithology, and rainfall—on landslides. The study uses numerical analysis to reveal the initiation mechanism of landslides. The research conclusions are as follows: The landslides within the study area are closely related to its natural topography, stratum lithology, and human activities. The majority of landslides are triggered by short-term extreme rainfall, while a smaller number are related to long-term continuous rainfall. The formation mechanism of landslides is primarily driven by dynamic water seepage, and the destruction process often lags behind the rainfall process. The conclusions can provide theoretical guidance for risk prevention and early warning of rainfall-induced landslides in the region.

Keywords: shallow landslide; extreme rainfall; influencing factors; damage mechanism

check for updates

Academic Editor: Wei Liu

Received: 13 January 2025
Revised: 2 February 2025
Accepted: 11 February 2025
Published: 12 February 2025

Citation: Li, Y.; Yan, E.; Xiao, W. Study on Shallow Landslide Induced by Extreme Rainfall: A Case Study of Qichun County, Hubei, China. *Water* **2025**, *17*, 530. https://doi.org/10.3390/w17040530

Copyright: © 2025 by the authors. Licensee MDPI, Basel, Switzerland. This article is an open access article distributed under the terms and conditions of the Creative Commons Attribution (CC BY) license (https://creativecommons.org/licenses/by/4.0/).

1. Introduction

Landslides are among the most destructive natural disasters worldwide, posing a grave threat to human life and property [1]. Controlled by the geological environmental conditions in different regions, the distribution of landslides presents regional characteristics. A large number of landslides induced by strong earthquakes are distributed in Yunnan and western Sichuan in China [2]. In the Three Gorges reservoir area and other reservoir areas, a large number of landslides affected by the fluctuation in reservoir water level are distributed [3]. A large number of loess landslides are distributed in northwestern China [4].

Rainfall has been identified as a primary catalyst for landslides [5]. In recent years, due to climate change, extreme rainfall events have become increasingly prevalent, resulting in a notable escalation in the number and frequency of landslides [6,7]. In China, Extreme rainfall triggered numerous landslides, causing substantial damage. For instance, on 21 July 2013, heavy rainfall triggered 976 shallow landslides in the Niangniangba Basin in China [8]. On 13 July 2020, a landslide of considerable magnitude occurred in Baima Town, Wulong District, Chongqing, resulting in significant damage to eight residential properties, two primary thoroughfares, one shale gas pipeline, and a substantial area

of agricultural land [9]. On 4 December 2020, a substantial landslide, precipitated by rainfall, occurred in Qingliu Village in southwestern China. This landslide resulted in the destruction of residential properties and infrastructure, including roads, and the formation of a barrier lake measuring approximately 100 m in length [10]. In mountainous regions, shallow landslides are typically initiated by short-term high-intensity rainfall events or by prolonged periods of low- to medium-intensity rainfall [11]. While the aforementioned landslides are typically characterized by minimal size, they have the potential to pose a significant threat to human settlements.

In their natural state, slopes typically experience an unsaturated condition. However, under conditions of extreme rainfall, the volumetric moisture content and saturation of the slope undergo rapid escalation [12]. As the amount of rainfall infiltration increases, the buoyancy pressure concomitantly rises [13]. Concurrently, the pore water pressure rises, the matric suction decreases, and the force balance of the slope is disrupted [14]. The interstitial spaces between soil particles are then filled with pore water, thereby reducing the stress between particles [15–17]. The effective stress of the rock and soil mass decreases, the shear strength decreases significantly, and the slope deforms [18,19]. The weakening of rock and soil mechanical parameters is influenced by rainfall infiltration, exhibiting an "S"-shaped change trend [20]. Yu X et al. [21] reproduced the parameter weakening and slope failure process, thereby confirming the hypothesis that water weakening induces landslides. Sun L et al. [22] took a water-weakened landslide as an example and proposed a stability evaluation method based on a double-sided progressive failure mechanism based on the staged saturated softening process of the sliding zone.

Rainfall-induced landslides are closely related to water seepage [23]. In the initial stages, the degree of rainfall intrusion can reach 70–80%, but it decreases exponentially as the duration of rainfall increases [24]. Furthermore, an increase in penetration depth has been shown to result in a concomitant decrease in infiltration rate. The hydrological response of slopes frequently exhibits characteristics of lagging behind changes in rainfall [25]. As the saturation of the slope increases, seepage parallel to the slope surface gradually forms [26], and the permeability points to the outside of the slope, increasing the possibility of slope failure [27]. The migration of soil particles in conjunction with the water flow [28] results in a modification of the slope particle grading [29,30], leading to the formation of one or more fast seepage channels within the slope. This, in turn, accelerates the transformation of the slope seepage field.

Rainfall-induced landslides are the result of a combination of factors, including water and geological environment. A substantial body of research has identified a correlation between landslide occurrence and various rainfall characteristics, such as intensity, duration, and antecedent precipitation [31,32]. Furthermore, a specific degree of hysteresis has been observed in the effect of rainfall on landslides [33]. The distinctive configuration of the slope itself exerts a pivotal influence on the genesis of rainfall-induced landslides. Research has demonstrated a negative correlation between slope angle and stability, under conditions of constant rainfall intensity [34]. The variation in rainfall intensity exerts a substantial influence on the sliding surface depth of non-cohesive slopes, and the soil bonding strength also affects the sliding surface depth [35]. Additionally, it has been established that the initial soil moisture content exerts a significant influence on the process of rainfall infiltration, thereby affecting the stability of the slope [36].

In recent decades, a substantial body of research has been conducted on the subject of rainfall-induced landslides. However, due to variations in geological and environmental conditions, as well as precipitation patterns that result in landslides, the existing conclusions may have certain limitations when applied to the study of landslides in an unknown new

area. And to the best of our knowledge, there has been no research conducted on shallow landslides induced by extreme rainfall in Hubei, China.

Therefore, the present study utilizes the landslides and daily rainfall data induced by multiple rounds of extreme rainfall in Qichun County in June and July 2016 as its research basis. The study analyzes the basic characteristics of extreme rainfall and landslides and explores the influence of five variables, namely altitude, slope, slope aspect, stratum lithology, and rainfall, on the formation of landslides. Utilizing the statistical analysis outcomes of the geological environmental influencing factors, a representative typical landslide was selected, and the numerical simulation method was employed to profoundly analyze the hydrological response process and stability change process in the landslide formation, unveiling the landslide formation mechanism. The objective of this research is twofold: first, to enhance the local understanding of such landslides, and second, to serve as a reference for local governments in the prevention of the risk of rainfall-induced shallow landslides. Additionally, the findings will contribute to the broader study of global rainfall-induced shallow landslides.

2. Study Area and Geological Environment Background

The study area under consideration is located in Qichun County, eastern Hubei Province, China (Figure 1a,b). The region's geographical limits extend from 115°12′ to 115°56′ east longitude and 29°59′ to 30°40′ north latitude (Figure 1c). The total area of the region is approximately 2397.6 km^2. The region's population is approximately 1.1 million.

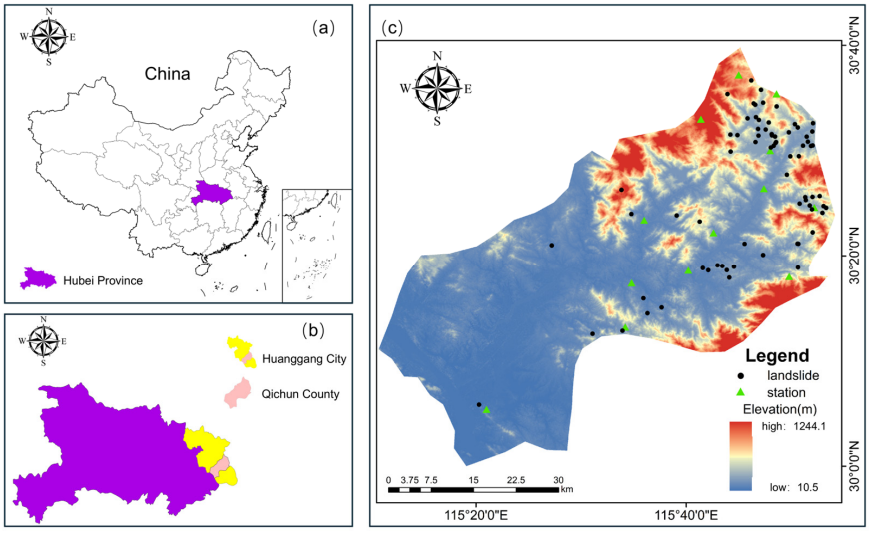


Figure 1. (**a**) Hubei Province, China, (**b**) Qichun County, Huanggang City, (**c**) topographic map of Qichun County.

The area is situated at the southern foot of the Dabie Mountains, which exhibit significant topographical variability, with elevations ranging from a maximum of approximately 1244.1 m to a minimum of about 10.5 m. The overall terrain exhibits a gradual incline from northeast to southwest, as illustrated in Figure 1c. The topography is marked by a diversity of landforms, including tectonic erosion medium and low mountains, tectonic erosion hills, denudation accumulation hillocks, and plains.

The stratigraphic ages in this area range from the Archean to the Cenozoic and consist of nearly 16 geological units. Table 1 presents the stratigraphic ages and their corresponding lithologies in the study area.

The study area boasts a complex geological structure, having experienced numerous tectonic movements. The most significant of these are the Dabie–Lüliang Movement, the

Yangtze Movement, and the Yanshan Movement. The Qinling east–west tectonic belt, the Huaiyangshan tectonic belt, and the Neocathaysian tectonic belt in eastern China comprise the primary geological tectonic systems within the control area. The region has demonstrated notable activity in tectonic processes, magmatic rock formations, metamorphism, and mixed lithification. Since the Quaternary System, the structure in the area has undergone an overall slow upward trend of uplift, accompanied by weathering and erosion.

Table 1. Description of the lithology of the formation.

Stratigraphic Age	Lithology Description
Archean–Proterozoic–Proterozoic Sinian System (Ar-Pt-Z_1)	Metamorphic rocks mainly include gneiss, schist, diabase, migmatite, etc. Igneous rocks are mainly gabbro and diabase.
Proterozoic Sinian System and Paleozoic Cambrian System (Z_2-$\in$)	Sedimentary rocks mainly include dolomite, limestone, and shale. Igneous rocks are mainly diorite, gabbro, and diabase.
Paleozoic Silurian (S)	Mainly mudstone, silty mudstone, and fine-grained sandstone.
Paleozoic Permian (P)	The sedimentary rocks are mainly limestone, siliceous rock, siliceous limestone, and flint limestone. Igneous rocks are mainly monzogranite, diorite, and quartz diorite.
Mesozoic Triassic, Jurassic, and Cretaceous (T-J-K)	Sedimentary rocks are mainly composed of purple siltstone, argillaceous siltstone, quartz sandstone, mudstone, fine sandstone, and conglomerate, interbedded with mudstone or shale. Igneous rocks are mainly biotite granite.
Cenozoic Quaternary (Q)	Mainly alluvial, residual slope accumulation, and landslide accumulation. Mainly sand, silty clay, gravel-containing sand, sandy gravel.

The study area is characterized by a subtropical continental monsoon climate. The mean annual temperature is 16.8 °C. The predominant wind directions during winter months are northeast and northwest, while in summer, the predominant wind directions are southeast and southwest. The annual average rainfall statistics of the study area from 2000 to 2019 (Figure 2a) demonstrate a conspicuous interannual variation in rainfall. The mean annual precipitation is 1287.9 mm, with a maximum of 1939.8 mm recorded in 2016 and a minimum of 968.3 mm in 2013. The multi-year monthly average rainfall statistics (Figure 2b) indicate a mean value of 121.53 mm, with a unimodal distribution characteristic and the maximum monthly average rainfall occurring in July. The annual rainfall data reveal a general trend of increased precipitation and decreased intensity in March and April, with a total annual rainfall of 675.8 mm, accounting for 46.34% of the annual precipitation, during the months of May to July. This period is characterized by higher intensity and more rainy days. In contrast, August and September exhibit a decrease in precipitation and intensity, with fewer rainy days and less intensity from October to January of the following year.

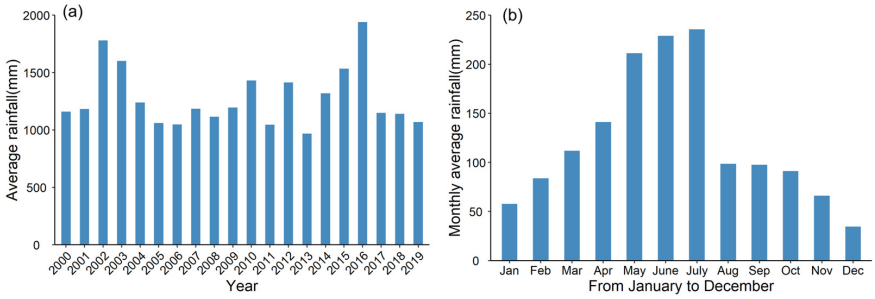


Figure 2. Precipitation statistics in the study area from 2000 to 2019: (**a**) annual average rainfall, (**b**) monthly average rainfall.

3. Materials and Methodology

3.1. Acquisition and Processing of Data

Due to the special topography and landforms, landslides occur every year in Qichun. In consequence of the precipitation experienced in June and July 2016, a considerable number of landslides occurred, an occurrence which was uncharacteristic of the region. In light of the disaster information reported by the local authorities, a field investigation was promptly conducted, encompassing the verification of the fundamental characteristics of the landslides and the disaster situation. A comparison of the data recorded at the time reveals that most landslides are accompanied by complete and detailed information. However, due to inherent issues with data collection methods and the temporal inconsistencies therein, the data set was found to be incomplete. To ensure the relative completeness and accuracy of the statistical analysis, 75 landslide events were selected as the research objects. To facilitate the statistical analysis, different influencing factors were graded (Table 2).

Table 2. Classification of different influencing factors.

Landslide Conditioning Factor	Category	Number of Landslides	Landslide Conditioning Factor	Category	Number of Landslides
Area (m^2)	[0, 100)	4	Volume (m^3)	[0, 100)	4
	[100, 300)	20		[100, 250)	12
	[300, 500)	17		[250, 500)	13
	[500, 700)	11		[500, 1000)	11
	[700, 1000)	6		[1000, 1500)	7
	[1000, 3000)	11		[1500, 3000)	6
	[3000, 6000)	3		[3000, 6000)	8
	[6000, 10,000)	1		[6000, 10,000)	5
	[10,000, 40,000]	2		[10,000, 30,000)	3
Slope (°)	[20, 25)	1		[30,000, 100,000)	3
	[25, 30)	5		[100,000, 1,000,000]	3
	[30, 35)	19	Thickness (m)	[0, 1)	5
	[35, 40)	9		[1, 2)	16
	[40, 45)	16		[2, 3)	25
	[45, 50)	8		[3, 4)	9
	[50, 55)	5		[4, 5)	3
	[55, 60)	2		[5, 6)	7
	[60, 65)	7		[6, 7)	0
	[65, 70]	3		[7, 8)	1
Aspect	N	5		[8, 9)	3
	NE	7		[9, 10)	1
	E	7		[10, 11)	3
	SE	15		[11, 30]	2
	S	18	Altitude (m)	[0, 100)	15
	SW	12		[100, 200)	48
	W	4		[200, 300)	7
	NW	7		[300, 400)	3
Stratigraphic age and lithology	Gneiss (Ar-Pt)	62		[400, 500)	1
	Granite ($\eta\gamma_5$)	13		[500, 600)	1

Due to the limitation of the degree of refinement of landslide data in 2016, the occurrence date can only be accurate to the day, and the hour of landslide occurrence cannot be accurately obtained. Consequently, this study will be based on daily rainfall. To this end, daily cumulative rainfall data from 0:00 to 24:00 in June and July of 2016 were obtained from

13 automatic rainfall monitoring stations within the study area (Figure 1c). To obtain the daily rainfall data for each landslide location, the landslide coordinates and the automatic rainfall monitoring station coordinates were matched with each other, with the shortest distance being used as the objective.

3.2. Methodology

The approach adopted in this study consists of two primary steps. Initially, statistical analysis was employed to ascertain the characteristics of rainfall-induced landslides and the relationship between landslides and their influencing factors in the study area, utilizing the landslide and rainfall data obtained from the field survey. Subsequently, based on the statistical outcomes, representative landslides were selected for detailed analysis. The Geostudio (version number 2022.1) software was utilized to investigate the seepage field and stability of landslides under rainfall conditions. Seepage analysis was conducted within the Seep/w module, while stability analysis was performed in the Slope/w module.

In analyzing the seepage process of landslide under rainfall conditions, the relevant theories were as follows:

(1) Darcy's law

Darcy's law was originally derived from saturated soil. Subsequently, it was determined that Darcy's law is also applicable to unsaturated soils. The formulation of Darcy's law is as follows:

$$v = \frac{Q}{A} = kJ = -k\frac{dH}{ds} \tag{1}$$

where v is the average flow velocity of the section, Q is the flow rate, A is the flow cross-sectional area perpendicular to the flow velocity direction, k is the permeability coefficient, and J is the permeability gradient.

(2) Two-dimensional seepage differential equation

The seepage differential equation is derived from the law of conservation of mass. The general control differential equation can be expressed as follows [37]:

$$\frac{\partial}{\partial x}(k_x\frac{\partial H}{\partial x}) + \frac{\partial}{\partial y}(k_y\frac{\partial H}{\partial y}) + Q = \frac{\partial \theta}{\partial t} \tag{2}$$

where k_x and k_y are the saturated permeabilities in the x and y directions, respectively, H is the total hydraulic head, Q is the applied boundary flow, θ is the water content per unit volume, and t is the time.

(3) van Genuchten model

The soil–water characteristic curve (SWCC) delineates the functional relationship between soil moisture content and suction. The van Genuchten model is a closed, smooth three-parameter model that was proposed by van Genuchten [38]. The expression is as follows:

$$\theta = \theta_r + \frac{\theta_s - \theta_r}{\left[1 + \left(\frac{u_a - u_w}{a}\right)^n\right]^m} \tag{3}$$

where a, m, n are nonlinear regression parameters, θ_s is the saturated volumetric water content, θ_r is the residual volumetric water content, u_a is the pore gas pressure, and u_w is the pore water pressure. The value range of the volumetric water content θ in the formula is $\theta \in (\theta_r, \theta_s]$. In unsaturated soil, the pore gas pressure is not equivalent to the pore water pressure, and $u_a > u_w$. The formation of matrix suction occurs when there is a pressure difference between the pore water and the pore gas within the soil.

In conjunction with seepage analysis, the safety factors for various durations of rainfall are calculated. The limit equilibrium method is usually used when performing safety factor calculations. The Morgenstern–Price method is a rigorous, rigid body limit equilibrium analysis technique [39] that can be utilized to assess the stability of landslides with sliding surfaces of any configuration. The method satisfies the balance of forces in the normal direction of the sliding surface and in the direction of the sliding surface, as well as the balance of moments about the midpoint of the bottom sliding surface. The calculation results obtained from this method are characterized by enhanced safety and reliability.

4. Event Description

4.1. Rainfall Characteristics

In June and July of 2016, Qichun experienced multiple rounds of continuous heavy rainfall, with a cumulative total of 878.7 mm, constituting 42.22% of the annual precipitation in 2016 (Figure 3a). This represented a substantial increase of 92.02% compared to the rainfall in the same period of the previous year (457.6 mm) and a significant increase of 120.52% over the multi-year average rainfall (398.46 mm) (Figure 3b). A review of monthly rainfall data indicates that the precipitation levels in June and July of 2016 were significantly atypical.

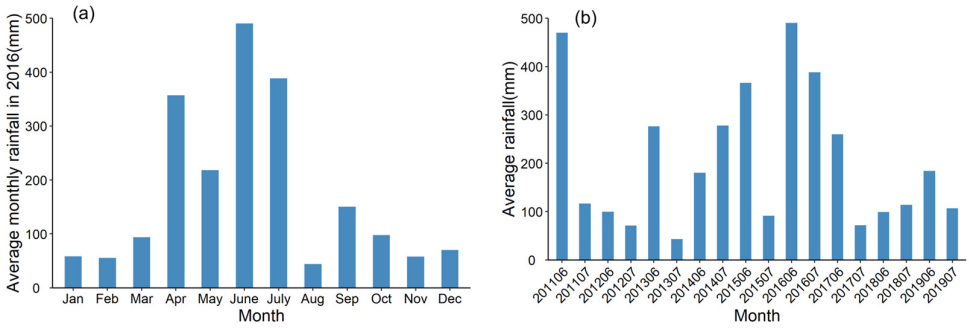


Figure 3. (**a**) The average monthly rainfall in 2016; (**b**) the average monthly rainfall in June and July from 2011 to 2019.

As demonstrated in Figure 4, from June to July, the daily precipitation exhibited an uneven distribution and significant variations. The maximum daily rainfall recorded on 2 July was 135.11 mm. During this interval, the region underwent three distinct phases of extreme rainfall events. The first occurred on 18 June, when the rainfall suddenly surged for two consecutive days. The total rainfall was about 155.6 mm, accounting for 16.61% of the total rainfall in June and July. The second occurrence, on 27 June, resulted in a total rainfall of approximately 99.38 mm, constituting 10.50% of the total rainfall in June and July. The third occurrence transpired on 30 June and persisted for a duration of seven days. The total precipitation in this interval exceeded 405.62 mm, constituting more than 43.30% of the total precipitation in June and July. The interval between the first and second extreme rainfall events was eight days, while the interval between the second and third extreme rainfall events was two days. A distinguishing feature of rainfall is the coexistence of continuous rainfall and multiple extreme rainfall processes. This rainfall process is rare in the region in terms of cumulative rainfall and the number of extreme rainfall events.

The data concerning precipitation from stations in disparate regions within the study area were selected for analysis (Figure 5). The stations were located in the northeast (Q9526), east (Q9525), central (Q9515), north (Q9514), and southwest (Q9518) of the area under study. The findings indicate that variations in rainfall were observed across different regions within the study area. The analysis indicates a predominant concentration of rainfall in

the eastern and northeastern regions, followed by the central, northern, and southwestern regions.

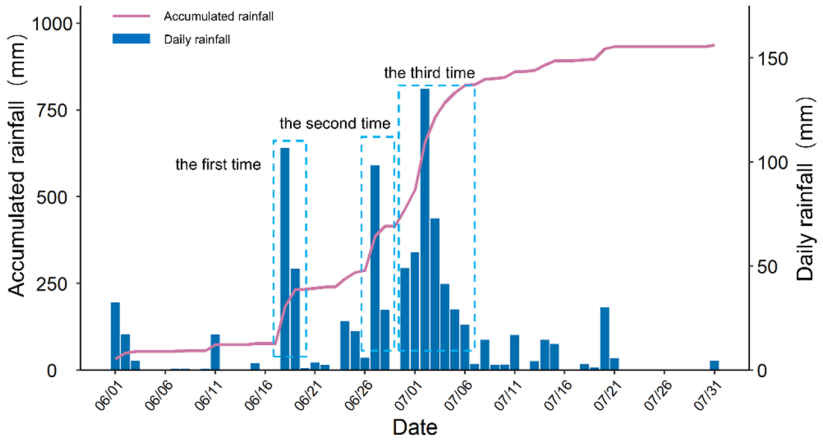


Figure 4. The average daily and cumulative rainfall at 13 rainfall monitoring stations from June to July 2016.

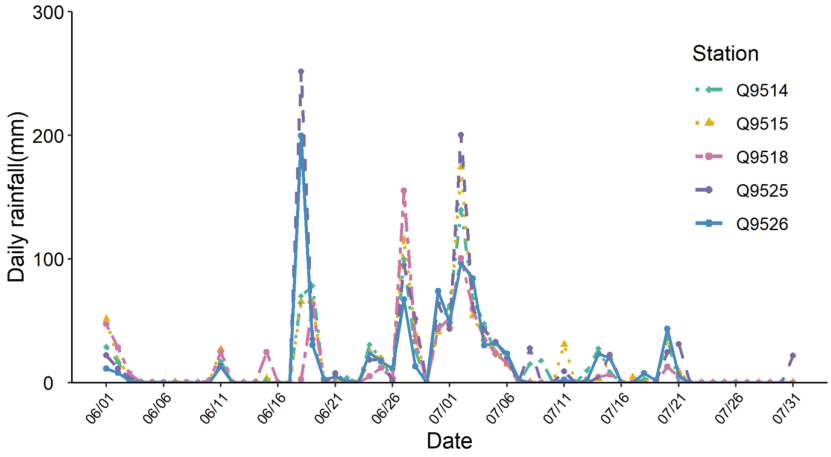


Figure 5. Comparison of daily rainfall at five different rainfall monitoring stations.

4.2. Development Law of Landslide

4.2.1. Spatial Distribution

Qichun County, which is composed of 15 townships, has experienced landslides in 12 of these townships. The landslides are characterized by their high number, widespread distribution, and relatively concentrated distribution, and their concentration within the Northeast region is pronounced (Figure 1c). The landslide distribution density undergoes a transition from strong to weak as it shifts from north to south and from east to west. This phenomenon is largely consistent with the observed distribution of rainfall, thereby underscoring the established correlation between landslides and precipitation.

4.2.2. Landslide Scale

According to the landslide volume, there are 72 small landslides (<100,000 m^3) and 3 medium landslides (100,000–1 million m^3) (Figure 6), accounting for 96% and 4% of the total landslides, respectively. These findings indicate that the landslides induced by this rainfall were predominantly small-scale.

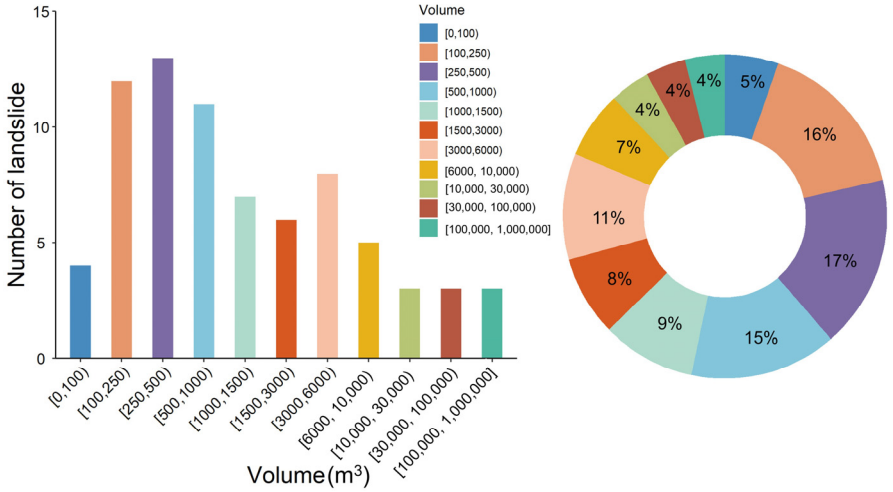


Figure 6. Landslide volume statistics.

The total landslide area is 121,868.5 m^2, with the largest landslide area measuring 36,000 m^2 and the smallest measuring 30 m^2. A total of 58 landslides with an area of more than 1000 m^2 were identified, constituting approximately 77% of the total number of landslides. In addition, 15 landslides with an area ranging from 1000 to 10,000 m^2 were documented, representing about 20% of the total number of landslides. Lastly, two landslides with an area exceeding 10,000 m^2 were noted, accounting for around 3% of the total number of landslides (Figure 7).

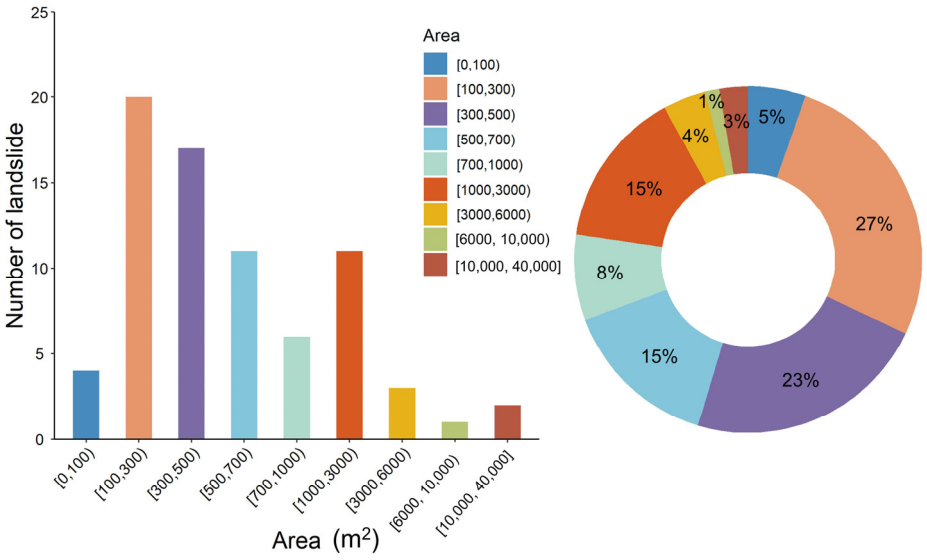


Figure 7. Statistics of landslide area.

4.2.3. Landslide Thickness

The distribution of landslides based on thickness can be categorized into two groups: 70 shallow landslides with a thickness of less than 10 m and 5 medium-thick landslides with a thickness greater than 10 m. These two categories account for 93% and 7% of the total landslides, respectively (Figure 8). The majority of landslides resulting from this precipitation were classified as shallow landslides, and the frequency of landslides exhibited an exponential decline when the thickness exceeded 3 m.

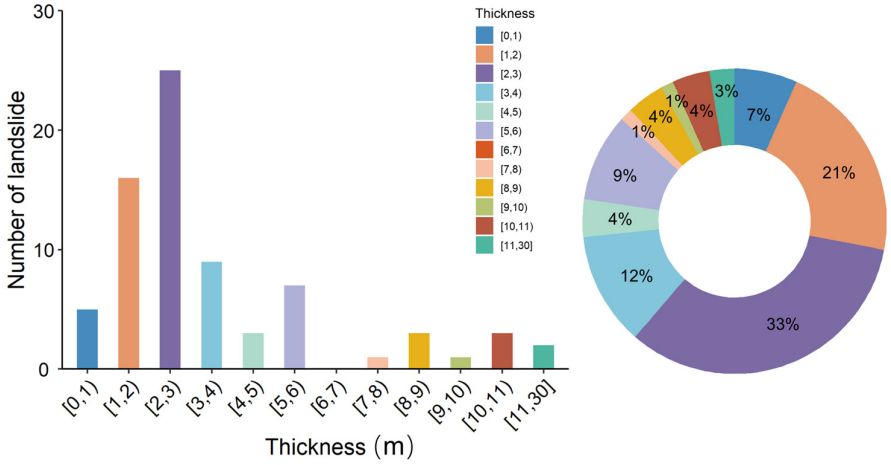


Figure 8. Thickness statistics of sliding body.

4.3. Disaster Severity

The substantial landslides resulted in significant damage or destruction to numerous residences, compromised the integrity of several thoroughfares, and led to fatalities (Figure 9). The landslides caused three fatalities, damaged over 40 residential properties, affected approximately 563 m of road infrastructure, and resulted in direct economic losses amounting to approximately RMB 4 million. Furthermore, the estimated threat to people is approximately 345, to houses at around 2639, and the potential economic loss is estimated to be approximately RMB 195 million.

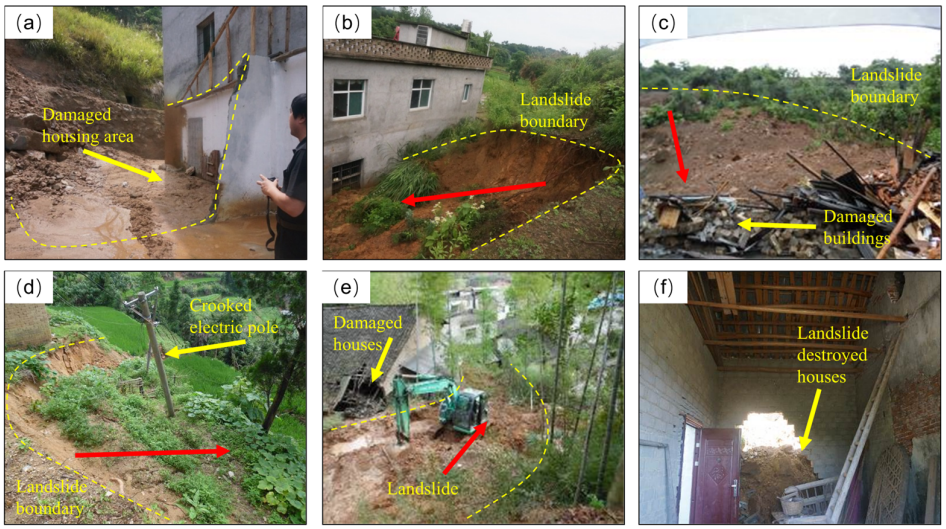


Figure 9. Disaster situation: (**a**) a house has been destroyed, (**b**) a house has been damaged, (**c**) a house has been destroyed, (**d**) an electric pole has been tilted, (**e**) a house has been damaged, (**f**) a house has been damaged.

5. Results of Influencing Factor Analysis

A variety of factors, including topography, stratum lithology, and rainfall, play a crucial role in the formation of landslides. The present study is an analysis of the relationship between various factors and landslides. This analysis is based on the acquisition of various topographic indicators, lithology information, and rainfall data.

5.1. Topography

Topographic conditions have been identified as a primary factor in landslide formation, exerting a substantial influence on the spatial and temporal distribution of landslides [40].

5.1.1. Altitude

The correlation between landslides and altitude is illustrated in Figure 10. The majority of landslides transpire in low-altitude regions, exhibiting a notable concentration at elevations ranging from 100 to 200 m above sea level. This phenomenon may be attributed to the intensive human activities in these regions, which include residential construction and road development. These activities disrupt the natural slope of the land, potentially leading to landslides. The rock and soil are highly exposed, and they are severely affected by weathering, which weakens their physical and mechanical properties. In the context of heavy rainfall, the stability of slopes in these areas is particularly vulnerable to degradation.

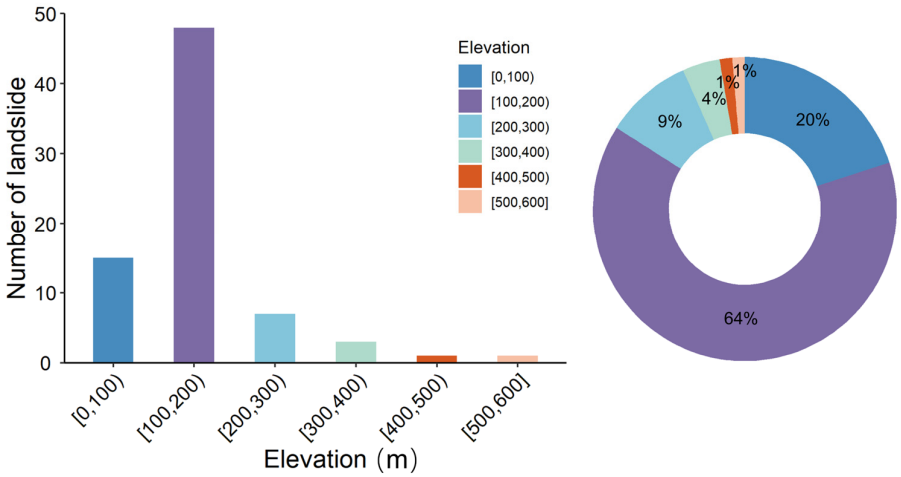


Figure 10. Number of landslides and altitude.

5.1.2. Slope

Slope affects the slope stress field, rainwater runoff, and material migration, thus serving as a pivotal factor in landslide assessment. The statistical analysis of the relationship between landslides and slopes (Figure 11) reveals a clear trend: the number of landslides increases initially and then decreases with increasing slope. Landslides with a gradient exceeding 50° are attributed to direct deformation and the subsequent destruction of high and steep slopes that have been formed by artificial slope cutting. The remaining landslides were formed due to artificial slope cutting, especially cutting at the slope foot, which formed an open surface at the front edge of the original slope. This provided favorable conditions for the sliding deformation of the slope. The slopes with original slopes that are more precipitous (30–45°) are the most affected, i.e., the most likely to slide. Conversely, the gentler the original slope, the less affected it is by artificial slope cutting, and the fewer landslides occur. This assertion is corroborated by statistical evidence.

5.1.3. Slope Aspect

The statistical relationship between landslide and slope aspect is illustrated in Figure 12. The predominant slope directions for landslide development are southeast (SE), south (S), and southwest (SW), with 15, 18, and 12 landslides, respectively, accounting for 20%, 24%, and 16% of the total landslides. This observation is consistent with the findings of previous studies, which have demonstrated a strong correlation between landslide distribution and slope direction [41]. This phenomenon may be attributed to variations in light exposure and vegetation distribution across different slope orientations. Shaded slopes exhibit higher levels of humidity and more substantial vegetation coverage, while sun-exposed slopes typically have sparse vegetation [42]. Sunny slopes are strongly influenced by dry–wet cycles, and the mechanical strength of rock and soil is weaker. Furthermore, anthropogenic activities, such as slope cutting and residential construction,

are frequently observed on south-facing slopes, driven by the desire to maximize sunlight exposure. Consequently, landslides are more prevalent on south-facing slopes.

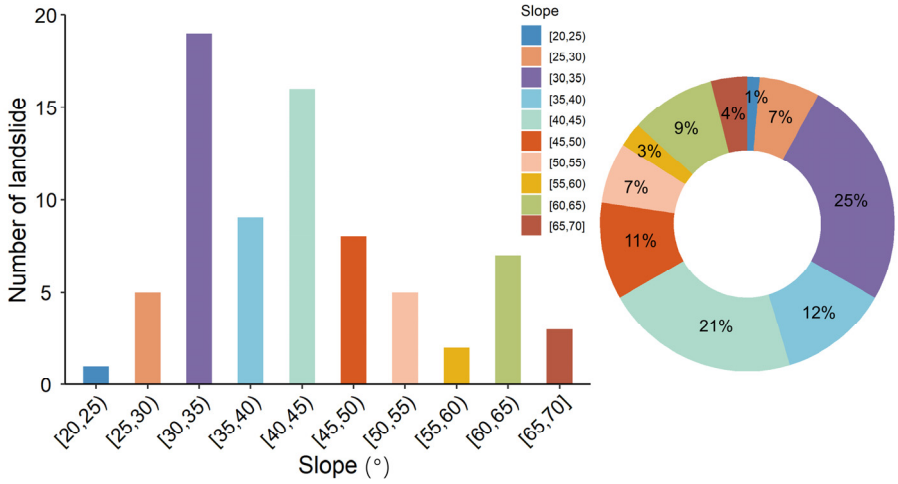


Figure 11. Number of landslides and slope.

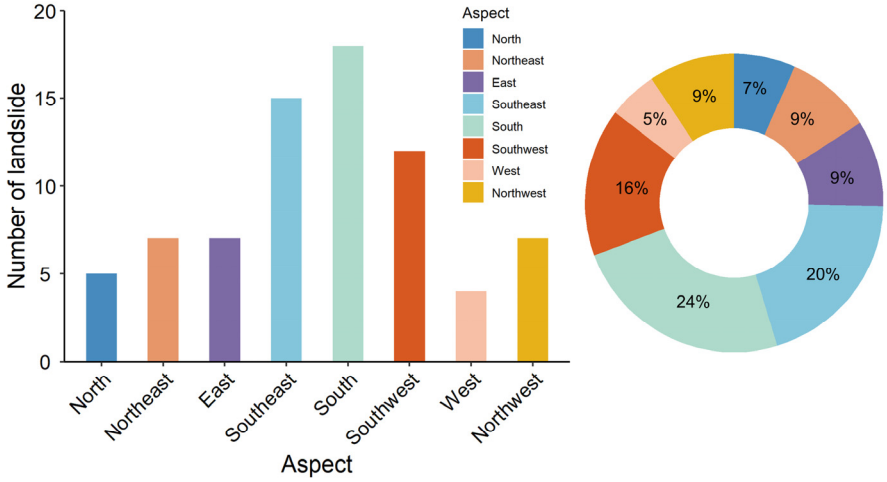


Figure 12. Number of landslides and slope direction.

5.2. Formation Lithology

Lithology is the material basis of landslides and has a controlling effect on them. Landslides occur in two main types of lithology (Figure 13). Here, 62 landslides occurred in various gneisses (Ar-Pt) formed by metamorphism and magmatism, with the majority occurring in metamorphic rocks such as biotite-plagioclase gneiss, granitic gneiss, and greisen gneiss. Further, 13 landslides occurred in biotite granite (ηγ5).

Metamorphic rocks, particularly gneiss, have been identified as the most slippery strata in the region. Within this category, landslides can be further classified into two distinct categories: soil landslides and rock landslides. In soil landslides, the landslide body consists mainly of silty clay and gravel with a loose structure, high porosity, and high permeability. The underlying gneiss has relatively high mechanical properties and relatively low permeability, and it is easy to form a slip surface at the base–cover interface. Gneiss has poor weathering resistance to rock landslides. As a result of artificial transformation, a severe weathering layer forms on the surface of the exposed rock slope. The rock mass is fractured, cracks develop, and the mechanical strength is low. Under the infiltration of rainfall, it is easy for a sliding surface to form along the strong and weak weathering contact surface.

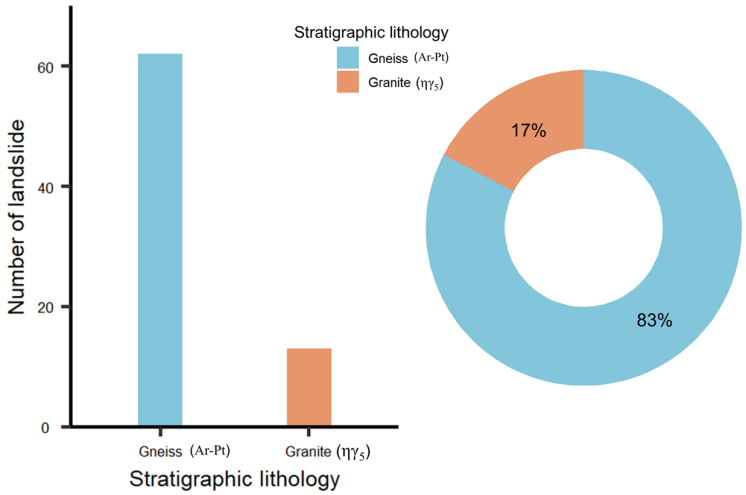


Figure 13. Landslides and different stratum lithology.

5.3. Rainfall

An analysis of the relationship between daily rainfall and the number of landslides in June and July of 2016 (Figure 14) revealed a correlation based on the 24 h rainfall grade classification standard (Table 3). The analysis indicates that four landslides occurred on days where heavy rain was recorded, with a probability of 50% on such days. In contrast, seven landslides transpired on days where rainstorms were observed, with a probability of 100% on these days. Further, 54 landslides occurred on heavy rain days, with a probability of 71% on heavy rain days; 3 landslides occurred on moderate rain days, with a probability of 22% on moderate rain days; 7 landslides occurred on light rain days, with a probability of 14% on light rain days; no landslides occurred on days with no rain or sporadic light rain.

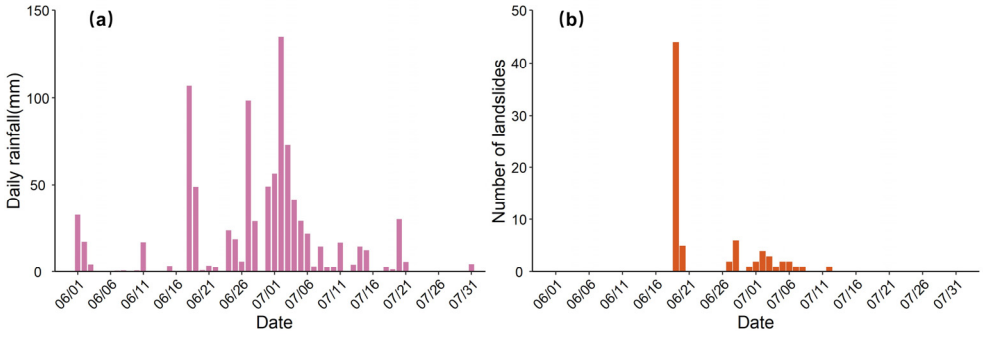


Figure 14. (**a**) Daily rainfall; (**b**) number of landslides per day.

Table 3. The 24 h rainfall classification standards and occurrence days.

Level Classification	24 h Cumulative Rainfall (mm)	Cumulative Days
no rain or scattered light rain	<0.1	18
light rain	0.1~9.9	22
moderate rain	10~24.9	9
heavy rain	25.0~49.9	7
torrential rain	50.0~99.9	3
extreme torrential rain	100.0~249.9	2

The results show that the precipitation that occurs on the day of the landslide plays a pivotal role in the landslide. The probability of landslide occurrence exhibited a positive correlation with the rainfall on the day of the landslide. However, given that one of the two days of extreme torrential rain coincided with the first day of extreme rainfall, the probability of landslide occurrence during the extreme torrential rain was 50% (18 June). The majority of landslides occur concurrently with heavy to torrential rains; however, a small number of landslides have also been observed to occur on light rain or rainless days after heavy rains, indicating a certain lag in the occurrence of landslides. On 18 June, the rainfall amounted to 106.83 mm, yet no landslides occurred, thereby substantiating this assertion.

The rainfall patterns that precipitate landslides can be categorized into two distinct types. The first type is characterized by the direct triggering of landslides by short-term heavy rainfall, a phenomenon exemplified by the heavy rainfall experienced on 18 and 19 June, which resulted in a significant number of slope deformations. The second type is associated with the combined effect of continuous accumulated rainfall and the rainfall that initiated the landslide, as observed in some landslides that occurred subsequent to 30 June.

In order to explore the landslide rainfall threshold and the relationship between accumulated rainfall days and landslide in the study area, Figure 15 was drawn. In the figure, 1 day of accumulated rainfall corresponds to the rainfall on the day of landslide occurrence, 2 days of accumulated rainfall corresponds to the rainfall on the day of landslide occurrence and the accumulated rainfall on the day before landslide occurrence, 3 days of accumulated rainfall corresponds to the rainfall on the day of landslide occurrence and the accumulated rainfall on the 2 days before landslide occurrence, and so on. The findings of the study indicate a positive correlation between the frequency of landslides and the amount of accumulated rainfall. The rate of increase in the number of landslides showed a gradual downward trend as the cumulative rainfall increased. The curve of the 1 day cumulative rainfall exhibits a substantial mutation at a cumulative rainfall of 25–50 mm, while the mutation points of the remaining curves are observed at cumulative rainfall levels of 250–300 mm. This finding indicates that when the accumulated rainfall reaches 250–300 mm, the majority of landslides in the study area have occurred. Furthermore, a substantial number of landslides may be triggered when the rainfall on that day reaches 25–50 mm.

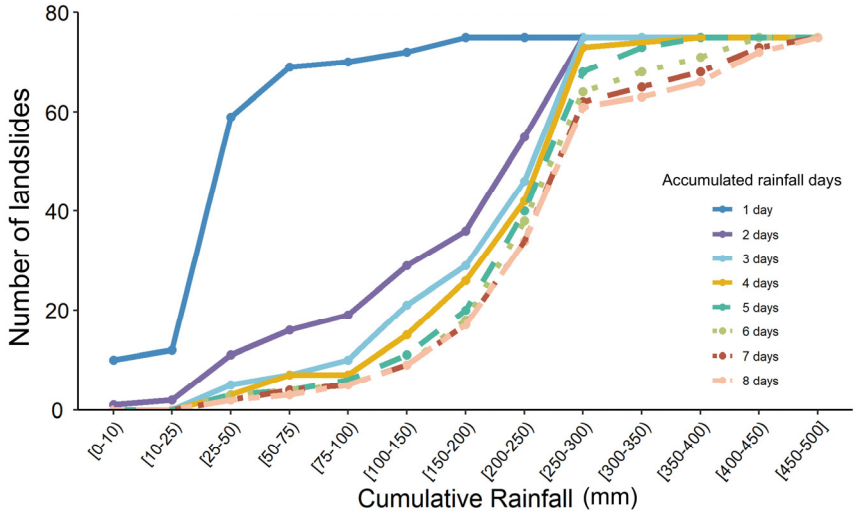


Figure 15. The relationship between the number of landslides and cumulative rainfall under different rainfall days.

It can also be observed that the mutation point gradually decreases with the increase in accumulated rainfall days. This indicates that some landslides require increased rainfall or longer rainfall periods for their destruction. A significant decrease in the mutation point is observed when the accumulated rainfall reaches five days, suggesting that the formation of landslides in the study area is more strongly influenced by the combined effect of the accumulated rainfall on the same day and the previous three days.

6. Results of Typical Rainfall-Induced Landslide Analysis

Due to the complexity and uncertainty inherent in landslides, conducting in-depth analyses of representative landslides can facilitate a more nuanced comprehension of the deformation and failure laws governing this particular type of landslide. Preliminary analysis indicates that landslides resulting from this precipitation are likely to occur on slopes with low altitudes, slopes ranging from 30 to 45°, and slope directions of SE, S, and SW, particularly in Archean–Proterozoic gneiss. The Pengshan Village Group landslide, which exhibits the aforementioned characteristics, was selected for further study from a total of 75 landslides. The temporal and spatial evolution of the seepage field within the landslide body was then studied, and the transient stability of the slope was analyzed.

6.1. Landslide Characteristics

On 3 July 2016, a minor soil landslide transpired in the vicinity of a residential structure in Pengshan Village, Zhangbang Town, northeastern Qichun County (Figure 16a). The landslide had a sliding direction of 115°, a width of 65 m, a length of 20 m, a thickness of 5 m, an area of 1300 m^2, and a volume of 6500 m^3. The sliding body was identified as Quaternary silty clay with gravel, characterized by a loose structure, a soil–rock ratio of 8:2, and a water content of 26.4%. The sliding surface corresponds to the contact between the strongly weathered gneiss and the Quaternary cover layer, with the sliding bed comprising strongly weathered granitic gneiss (Ar-Pt).

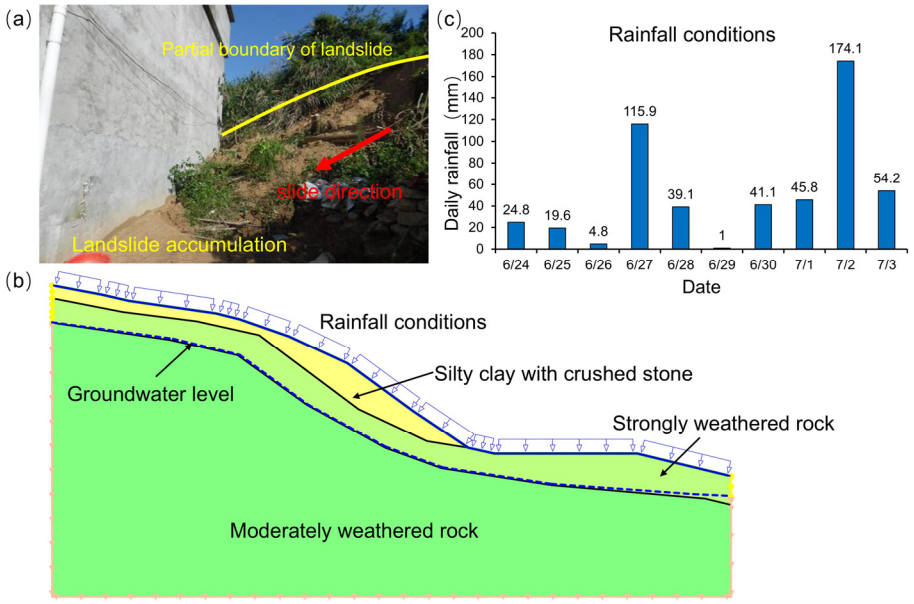


Figure 16. (**a**) Landslide deformation and damage, (**b**) 2D slope model, (**c**) rainfall conditions.

6.2. Model Building

According to the results of the geological survey, the landslide's primary sliding surface was designated as the calculation section, and a two-dimensional model was developed (Figure 16b). The grid division was based on a unit size of 1 m, and the majority of the

calculation units were quadrilateral, with a smaller number of triangular units in local areas. The total number of units and nodes that were divided was 1049 and 1116, respectively. The lowermost portion of the slope is delineated as an impermeable boundary, the areas beneath the groundwater level on both sides of the slope are designated as impermeable boundaries, the areas above the groundwater level are designated as free seepage boundaries, and the slope surface is delineated as a rainfall infiltration boundary. To account for the combined effects of previous continuous rainfall and the rainfall stimulated on the day of the landslide, the measured daily rainfall from 24 June to 3 July was selected as the rainfall boundary condition (Figure 16c). The recommended values for the calculation parameters of each slope layer were determined based on the on-site damage situation, indoor tests, back analysis, and similar landslide examples (Table 4).

Table 4. Recommended values of rock and soil parameters.

Rock and Soil Layer	Density (kg/m^3)	Cohesion (c/Kpa)	Internal Friction Angle (Φ/°)	Saturated Permeability Coefficient (m/d)	Maximum Degree of Water Saturation
Silty clay with gravel	2100	13	15	0.530000	0.35
Strongly weathered rock	2230	22.4	22	0.047347	0.25
Medium weathered rock	2560	25.6	35.2	0.002592	0.22

6.3. Pore Water Pressure

The initial pore water pressure of the slope is distributed linearly along the elevation, with positive values below the groundwater level and negative values above the groundwater level (Figure 17a). Following a period of four days of rainfall (from the 24th to the 27th), a significant increase in the slope's pore water pressure was observed. The most pronounced changes were observed in the upper and lower regions of the slope, accompanied by a shift in the direction of seepage, and the seepage direction became consistent with the slope deformation direction (Figure 17b). This observation indicates that early continuous rainfall exerts a substantial influence on the seepage field within the slope. On the sixth day, the pore water pressure of the slope became positive, and the seepage effect became intense (Figure 17c). On the 7th day, a decline in the pore water pressure within the shallow layer of the slope was observed (Figure 17d). This decline was attributed to a significant decrease in rainfall the previous day, accompanied by the ongoing seepage of rainwater from the slope. Subsequent to the continuation of the rainfall, a resurgence in pore water pressure was observed on the 8th day, with the moisture in the slope progressively amassing towards the toe of the slope under the influence of the hydraulic gradient (Figure 17e). On the 10th day, the unstable seepage of water in the overburden layer became more intense (Figure 17f), ultimately resulting in slope deformation and failure.

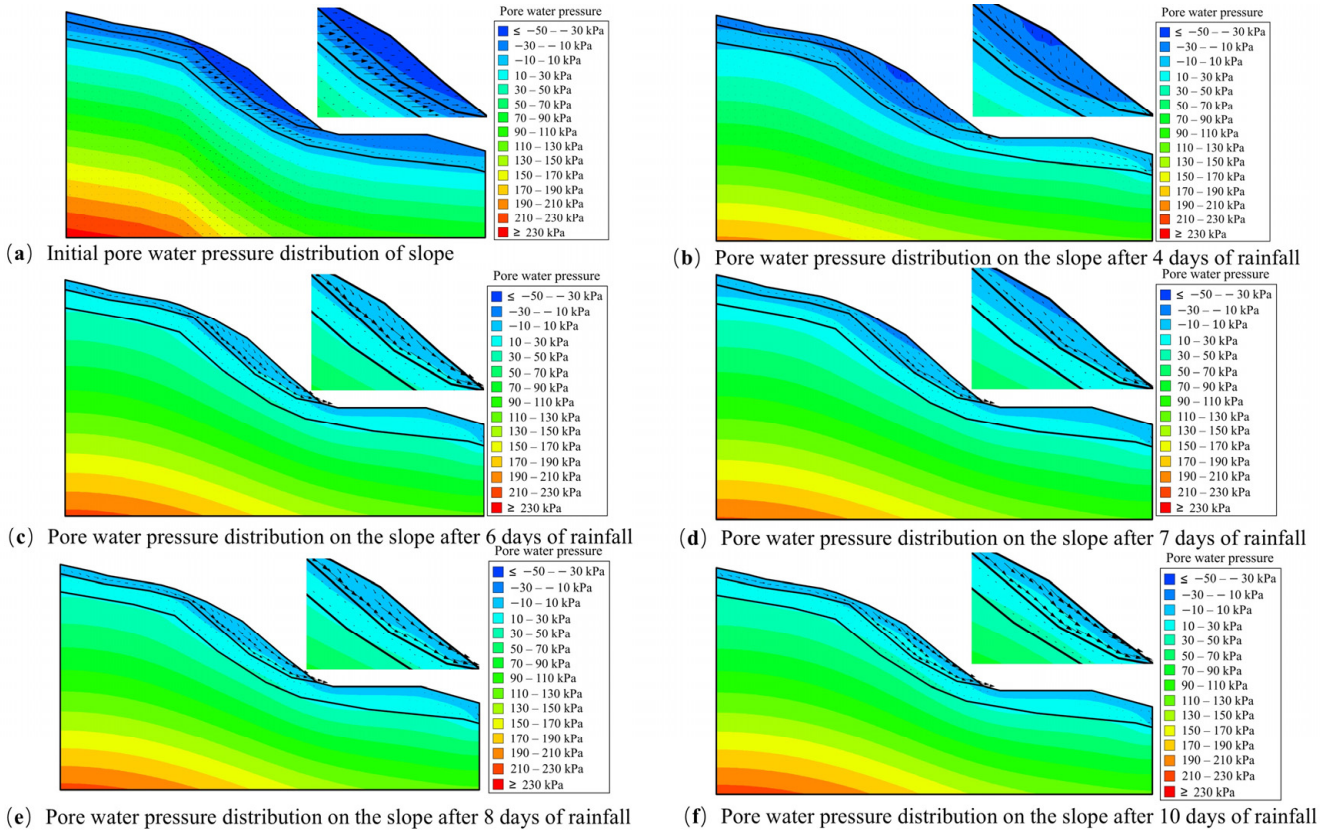


Figure 17. The variations in pore water pressure: (**a**) initial, (**b**) 4th day, (**c**) 6th day, (**d**) 7th day, (**e**) 8th day, (**f**) 10th day.

6.4. Saturation

Initially, the sliding body is in an unsaturated state (Figure 18a). In the context of persistent precipitation, there was an observed increase in the water content. Concurrently, the saturated area underwent expansion, and the infiltration line exhibited a gradual ascent (Figure 18b). The presence of a thin Quaternary cover layer at the slope's summit, coupled with the incessant percolation of rainwater into the slope's base, resulted in the initial manifestation of saturated areas at the slope's summit and base. On the 6th day, as the rainfall duration increased, the sliding body exhibited a tendency to become saturated from deep to shallow (Figure 18c). The decrease in rainfall on the previous day led to a reduction in rainfall infiltration. However, the water in the slope continued to infiltrate to the foot of the slope, resulting in the expansion of the unsaturated area in the sliding body on the 7th day (Figure 18d). On the 8th day, the range of the saturated area expanded once more, and the infiltration area increased further (Figure 18e). By the 10th day, the slope had become almost fully saturated, as depicted in Figure 18f.

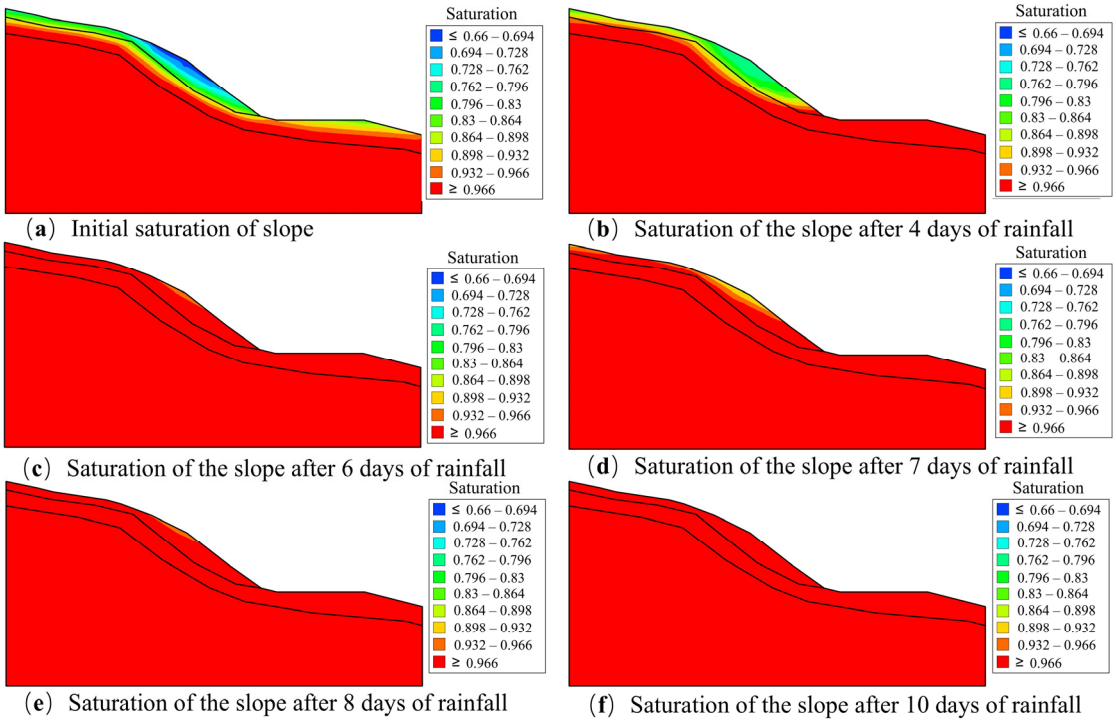


Figure 18. The variations in saturation: (**a**) initial, (**b**) 4th day, (**c**) 6th day, (**d**) 7th day, (**e**) 8th day, (**f**) 10th day.

6.5. Stability

The variation curve of the slope safety factor (Figure 19) was plotted to study the change in landslide stability with rainfall. The results indicate that the slope was in a stable state at the beginning of the simulation. Under the initial continuous rainfall, the slope safety factor remained constant, indicating that the early rainfall had no direct effect on the slope stability. However, on the fifth day, the factor of safety (FOS) began to decrease, and on the sixth day, it dropped sharply by 8%. On the 7th day, the curve exhibited an inflection point, indicating a transition in the slope stability trend. Beginning on the eighth day, with the reappearance of rainfall, FOS exhibited a consistent decline, reaching a 5%, 4%, and 3% decrease, respectively. By the 10th day, FOS had reached its nadir of 0.952, and the slope became unstable, resulting in damage.

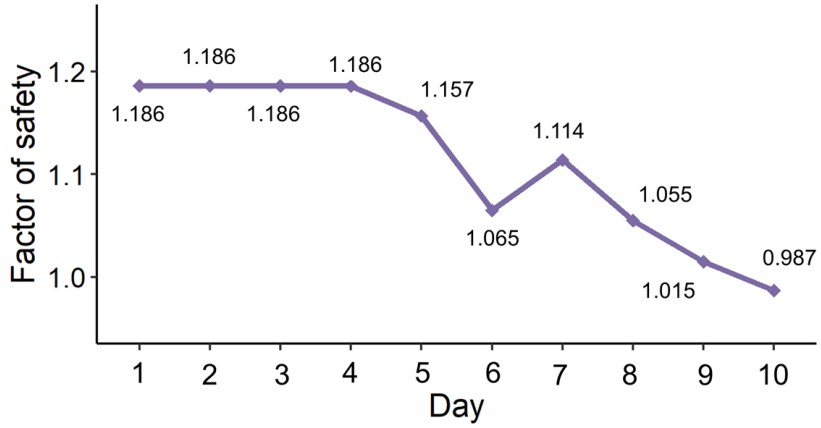


Figure 19. Changes in slope stability coefficient over time.

7. Discussion

7.1. Landslide Characteristics

This study is an inaugural evaluation of clustered landslides triggered by extreme rainfall events in Qichun County. The majority of the landslides were characterized by their small size, shallow depth, and rapid movement. This finding is consistent with the observations from analogous events documented worldwide [43,44], suggesting that anomalous or extreme rainfall events can precipitate shallow landslides in particular geographical locations.

Rainfall-induced landslides exhibit discernible clustering characteristics [45]. In regions exhibiting analogous geological and environmental characteristics, the occurrence of precipitation that exceeds the designated landslide rainfall threshold is conducive to the initiation of numerous landslide disasters. The statistical analysis results indicate that landslides in Qichun County are most likely to occur at elevations ranging from 100 to 200 m, with slopes measuring between 30 and 45 degrees, and a slope aspect facing either the SE, SW, or NE direction. The formation lithology comprises Archean Proterozoic gneiss. These results differ from those observed in other regions, which renders the findings highly pertinent to the local area. Consequently, in subsequent landslide risk management initiatives, a strategic focus on slopes exhibiting these specific geological characteristics is imperative.

The distribution of landslides is essentially congruent with that of rainfall. In the presence of substantial precipitation, the likelihood of landslides is concomitantly elevated. A variety of extreme rainfall events have the capacity to influence the formation of landslides. A significant proportion of landslides are influenced by short-term extreme rainfall events. However, it is important to acknowledge that landslides can also occur at times that are not synchronized with the occurrence of the heaviest rainfall [46]. It is imperative to acknowledge that continuous rainfall is another important factor that triggers landslides. The formation of such landslides is the result of the combined effect of previous accumulated rainfall and rainfall on the day of occurrence.

This landslide disaster also exhibited another salient characteristic: human engineering activities provided favorable conditions for landslides [47]. Landslides resulting from rainfall do not occur on natural slopes; rather, they occur on artificial slopes that have been modified by human activities. In the context of comparable geological environments and rainfall conditions, slopes that remained undisturbed by human activity did not undergo landslides. The construction of residential buildings and transportation infrastructure has resulted in alterations to the original topography of the hillside, thereby disrupting the equilibrium of the hillside. This led to stress adjustment and the formation of stress concentration at the slope's front end. Local residents exhibited a lack of awareness concerning landslide risk management. The majority of these slopes lacked proper protective measures, or even the most rudimentary ones, after excavation, which could not adequately compensate for or restore the original equilibrium state of the slope. The integrity of the rock and soil was compromised. The probability of landslides was greatly increased due to the long-term effects of physical weathering, particularly in conditions of extreme rainfall.

7.2. Failure Mechanism

Through numerical analysis, it was determined that rainfall exerts a significant influence on the landslide seepage field. In the initial phase of rainfall, the landslide mass is in an unsaturated state. As rainwater infiltrates the slope, the water content of the landslide mass increases, and the pore water pressure rises, gradually transitioning from an unsaturated state to a saturated state. The seepage field undergoes a substantial transformation upon the failure of a landslide in comparison with its initial state. Given the transient nature of

this phenomenon, changes in the seepage field within a landslide often lag behind changes in rainfall [48]. On the sixth day, the recorded rainfall was only 1 mm, and the pore water pressure and saturation did not demonstrate a downward trend but continued to increase. On the 7th day, a total of 41.1 mm of rainfall were recorded, accompanied by a decline in pore water pressure and saturation. This discrepancy is attributable to the intrinsic time lag between rainfall and its ensuing infiltration, resulting in delayed responses in the seepage field relative to variations in rainfall. This is particularly evident during the nascent stage of rainfall when the slope is in an unsaturated state and the soil permeability coefficient is low, impeding the swift infiltration of rainwater. This phenomenon is also supported by statistical data. While landslides were not observed during the heavy rain on the 18th, a significant number of landslides occurred on the 19th.

It has been observed that the safety factor remains consistent during the initial phase of rainfall. This phenomenon can be attributed to the fact that, in the initial stage of rainfall, the unsaturated area within the slope is substantial, and the permeability coefficient is significantly lower than the saturated permeability coefficient. This phenomenon can be attributed to the impact of matrix suction, which impedes the rapid infiltration of rainwater within a constrained time frame. Consequently, the seepage field undergoes relatively minor alterations over time. In general, the change response of the early stability lags far behind the changes in rainfall and seepage field. During this process, the bulk density of the slope increases, the sliding force increases, and the buoyancy increases. These changes have been shown to have an adverse effect on the stability of the slope. At this time, the anti-sliding force remains significantly greater than the sliding force. This observation indicates that hydrostatic pressure and buoyancy do not act as the primary factors that induce landslides. However, this phenomenon may also be attributed to the temporal requirement for the deterioration of the mechanical properties of the rock and soil.

The attenuation of slope stability is primarily observed in the latter half of the rainfall process, during which the change in the safety factor tends to be consistent with the change in the seepage field, albeit lagging behind the change in rainfall. This is due to the gradual saturation of the slope with rainwater as the rainfall continues, resulting in accelerated rainwater infiltration. The hydraulic gradient in the slope increases, the rainwater seepage is enhanced, and the seepage direction is consistent with the sliding direction (Figure 20), pulling the rock and soil to move. In this process, the slope stability is mainly affected by the driving effect of dynamic water seepage; however, the combined effect of long-term hydrostatic pressure and buoyancy cannot be ruled out.

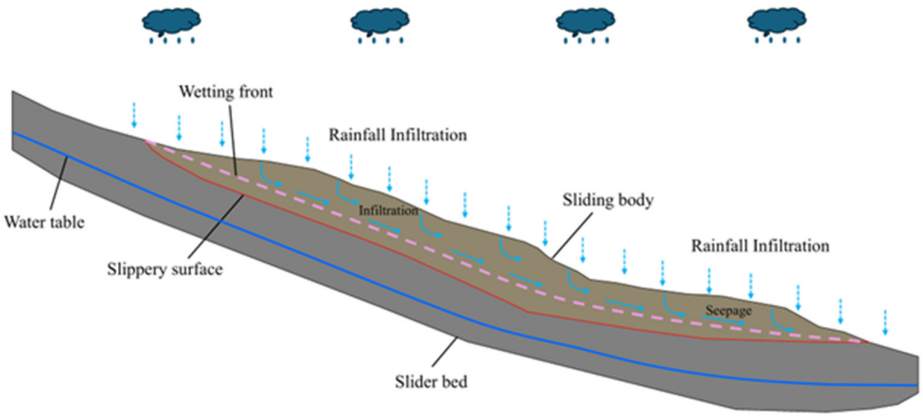


Figure 20. Rainfall seepage damage to shallow landslide.

The alteration in the safety factor is indicative of the progression of slope damage during the occurrence of rainfall. The continuous precipitation that transpired in the initial

four days prior to the formation of the landslide resulted in a substantial reduction in the safety factor, thereby ultimately compromising the critical state of slope stability and leading to the formation of a landslide. This finding is in alignment with the statistical outcomes that indicate the landslide was predominantly influenced by the rainfall on that specific day and the cumulative rainfall in the preceding three days.

It is reasonable to hypothesize that extreme rainfall events will become more prevalent in the future [49]. Concurrently, the frequency of rainfall-induced landslides is anticipated to escalate, their spatial distribution may undergo alterations, and the population at risk is expected to rise [50]. It is imperative to give full consideration to these changes in rainfall and to redouble our efforts to study the impact of extreme rainfall on landslides. This will allow us to prepare for possible disasters in advance and to avoid losses as much as possible.

8. Conclusions

This paper analyzes the fundamental characteristics and rainfall characteristics of landslides induced by multiple rounds of extreme rainfall in Qichun County in June and July 2016. It explores the effects of five variables on landslides: namely, altitude, slope, slope aspect, stratum lithology, and rainfall. The study reveals the formation mechanism of rainfall-induced landslides by taking a typical landslide as an example. The following four insights were obtained:

(1) The statistical analysis of landslides reveals that rainfall-induced landslides are predominantly small and shallow. The landslides are characterized by their high number, widespread distribution, and relatively concentrated distribution. The landslide incidence is higher in the north and east, and less frequent in the southwest. This variation is attributed to the distinct topographical features and human activity patterns within the study area.

(2) Landslides have been observed to occur most frequently on slopes with low altitudes, slopes of 30–45°, and slope directions of SE, S, and SW. These terrain conditions are closely related to human engineering activities, such as the construction of residential structures, and transportation infrastructure. This correlation is a primary factor that contributes to the high number of casualties and substantial property losses observed in landslide-affected areas. The occurrence of landslides is predominantly observed in metamorphic rock regions, with a lower frequency in igneous rock areas.

(3) Landslides are influenced by two distinct patterns of rainfall: the first is characterized by short-term extreme rainstorms, and the second is the combined effect of continuous accumulated rainfall and rainfall on the day that landslides occur. The threshold for rainfall on the day of most landslides is 20–50 mm, and the threshold for accumulated rainfall over multiple days is 250–300 mm. To enhance the efficacy of landslide prevention strategies, a focus on the day of rainfall and the accumulated rainfall over the previous three days is imperative.

(4) The primary factors contributing to landslides can be categorized into two primary factors: the artificial modification of slope topography, which serves as the fundamental control, and the occurrence of extreme rainfall, which functions as the triggering effect. The slope failure mechanism is predominantly driven by dynamic water seepage.

Author Contributions: Conceptualization, E.Y.; methodology, Y.L.; writing—original draft, Y.L.; writing—review and editing, W.X.; supervision, W.X.; funding acquisition, E.Y. All authors have read and agreed to the published version of the manuscript.

Funding: This research was funded by the National Natural Science Foundation of China (Grant No. 41972289).

Data Availability Statement: All data that support the findings of this study are available from the corresponding author upon reasonable request.

Acknowledgments: The authors thank the Third Geological Brigade of Hubei Province and the Huanggang Meteorological Bureau for providing the landslide data and daily rainfall data, respectively. First author acknowledges the financial support of the China Scholarship Council (CSC:202306410190) for supporting his research at the University of Salerno. We would like to thank all staff members who contributed to this study who are not named here.

Conflicts of Interest: The authors declare no conflicts of interest.

References

1. Das, S.; Sarkar, S.; Kanungo, D.P. Rainfall-induced landslide (RFIL) disaster in Dima Hasao, Assam, Northeast India. *Landslides* **2022**, *19*, 2801–2808. [CrossRef]
2. Zou, Y.; Qi, S.; Guo, S.; Zheng, B.; Zhan, Z.; He, N.; Huang, X.; Hou, X.; Liu, H. Factors controlling the spatial distribution of coseismic landslides triggered by the Mw 6.1 Ludian earthquake in China. *Eng. Geol.* **2022**, *296*, 106477. [CrossRef]
3. Zou, Z.; Tang, H.; Criss, R.E.; Hu, X.; Xiong, C.; Wu, Q.; Yuan, Y. A model for interpreting the deformation mechanism of reservoir landslides in the Three Gorges Reservoir area, China. *Nat. Hazards Earth Syst. Sci.* **2020**, *21*, 517–532. [CrossRef]
4. Hu, S.; Qiu, H.; Wang, N.; Wang, X.; Ma, S.; Yang, D.; Wei, N.; Liu, Z.; Shen, Y.; Cao, M.; et al. Movement process, geomorphological changes, and influencing factors of a reactivated loess landslide on the right bank of the middle of the Yellow River, China. *Landslides* **2022**, *19*, 1265–1295. [CrossRef]
5. Minder, J.R.; Roe, G.H.; Montgomery, D.R. Spatial patterns of rainfall and shallow landslide susceptibility. *Water Resour. Res.* **2009**, *45*, W04419. [CrossRef]
6. Moreiras, S.M. Climatic effect of ENSO associated with landslide occurrence in the Central Andes, Mendoza Province, Argentina. *Landslides* **2005**, *2*, 53–59. [CrossRef]
7. Zieher, T.; Gallotti, G.; Rianna, G.; Reder, A.; Pfeiffer, J. Exploring the effects of climate change on the water balance of a continuously moving deep-seated landslide. *Nat. Hazards* **2023**, *115*, 357–387. [CrossRef]
8. He, J.; Qiu, H.; Qu, F.; Hu, S.; Yang, D.; Shen, Y.; Zhang, Y.; Sun, H.; Cao, M. Prediction of spatiotemporal stability and rainfall threshold of shallow landslides using the TRIGRS and Scoops3D models. *Catena* **2021**, *197*, 104999. [CrossRef]
9. Zhou, C.; Huang, W.; Ai, D.; Xu, H.; Yuan, J.; Kou, L.; Luo, X. Catastrophic landslide triggered by extreme rainfall in Chongqing, China: July 13, 2020, Niuerwan landslide. *Landslides* **2022**, *19*, 2397–2407. [CrossRef]
10. Xue, D.; Dai, C.; Wu, Y.; Chen, K.; Tang, J.; Zhang, S. A catastrophic rainfall-induced high landslide, occurred on December 4, 2020, in the Qingliucun mountainous area of Southwest China. *Landslides* **2023**, *20*, 2187–2197. [CrossRef]
11. Jug, J.; Grabar, K.; Bek, A.; Strelec, S. Stabilization of Shallow Landslides Induced by Rainwater Infiltration—A Case Study from Northern Croatia. *Geotechnics* **2024**, *4*, 242–263. [CrossRef]
12. Tan, Y.L.; Cao, J.J.; Xiang, W.X.; Xu, W.Z.; Tian, J.W.; Gou, Y. Slope stability analysis of saturated–unsaturated based on the GEO-studio: A case study of Xinchang slope in Lanping County, Yunnan Province, China. Environ. *Earth Sci.* **2023**, *82*, 322. [CrossRef]
13. Yu, L.; Yan, C.; Guo, S.; Li, H.; Tan, J.Z.; Liu, G.; Xu, C.H.; Liu, Y. Mechanism analysis of Zulongding landslide on gentle piedmont slope: A creeping landslide triggered by rainfall. *Nat. Hazards* **2023**, *118*, 1211–1234. [CrossRef]
14. Wang, H.; Jiang, Z.; Xu, W.; Wang, R.; Xie, W. Physical model test on deformation and failure mechanism of deposit landslide under gradient rainfall. *Bull. Eng. Geol. Environ.* **2022**, *81*, 66. [CrossRef]
15. Sengani, F.; Mulenga, F. Influence of rainfall intensity on the stability of unsaturated soil slope: Case Study of R523 road in Thulamela Municipality, Limpopo Province, South Africa. *Appl. Sci.* **2020**, *10*, 8824. [CrossRef]
16. Yu, S.; Ren, X.; Zhang, J. Using an improved SPH algorithm to simulate thermo-hydro-mechanical-damage coupling problems in rock masses. *Case Stud. Therm. Eng.* **2023**, *47*, 103085. [CrossRef]
17. Yu, S.; Zhou, Y.; Yang, J.; Chen, W. Hydraulic fracturing modelling of glutenite formations using an improved form of SPH method. *Geoenergy Sci. Eng.* **2023**, *277*, 211842. [CrossRef]
18. Wang, S.; Demisa, M.G.; Han, B.; Hou, Q.; Zhang, Z. A material point method analysis of failure mechanism and kinematic behavior of rainfall-induced landslide. *Nat. Hazards* **2024**, *120*, 13875–13897. [CrossRef]
19. Zhong, W.; Zhu, Y.; He, N. Physical model study of an intermittent rainfall-induced gently dipping accumulation landslide. *Water* **2022**, *14*, 1770. [CrossRef]
20. Zhou, Z.; Shen, J.; Tang, S.; Duan, W.F.; Wang, J.Y.; Yang, R.C.; Zheng, S.Z.; Guo, F.L. Analysis of weakening law and stability of sliding zone soil in thrust-load-induced accumulation landslides triggered by rainfall infiltration. *Water* **2021**, *13*, 466. [CrossRef]
21. Yu, X.; Zhao, T.; Gong, B.; Tang, C.A. The water weakening effect on the progressive slope failure under excavation and rainfall conditions. *Bull. Eng. Geol. Environ.* **2024**, *83*, 316. [CrossRef]

22. Sun, L.; Li, C.; Shen, F. Two-surface progressive failure mechanism and stability quantitative evaluation of water-induced weakening retrogressive landslides: Case study for clay landslides, China. *Bull. Eng. Geol. Environ.* **2022**, *81*, 382. [CrossRef]
23. Chen, H.-E.; Chiu, Y.-Y.; Tsai, T.-L.; Yang, J.-C. Effect of Rainfall, Runoff and Infiltration Processes on the Stability of Footslopes. *Water* **2020**, *12*, 1229. [CrossRef]
24. Zhen, J.; Yang, X.; Wang, B.; Fan, H.; Meng, M. Study on the destruction of backfilled loess slopes by short-term extreme rainfall erosion. *Bull. Eng. Geol. Environ.* **2023**, *82*, 406. [CrossRef]
25. Wang, T.; Liu, F.; Yu, Y.; Cai, H. Numerical analysis of hydrological response in loess excavation and filling area under multi-year precipitation infiltration. *Bull. Eng. Geol. Environ.* **2023**, *82*, 372. [CrossRef]
26. Paronuzzi, P.; Bolla, A. Rainfall infiltration and slope stability of alpine colluvial terraces subject to storms (NE Italy). *Eng. Geol.* **2023**, *323*, 107199. [CrossRef]
27. Guo, Z.; Huang, Q.; Liu, Y.; Wang, Q.; Chen, Y. Model experimental study on the failure mechanisms of a loess-bedrock fill slope induced by rainfall. *Eng. Geol.* **2023**, *313*, 106979. [CrossRef]
28. Zhang, Z.; Sheng, Q.; Song, D.; Fu, X.; Zhou, Y.; Huang, J. Stability evaluation of the high fill deposit slope subjected to rainfall considering water deterioration. *Bull. Eng. Geol. Environ.* **2023**, *82*, 68. [CrossRef]
29. Wei, S.-W.; Lv, S.; Jiang, J.-J.; Cai, D.-G.; Cui, Z.-D. Similarity Model Test on Rainfall Scouring Mechanism of High-Speed Railway Subgrade Slope. *Appl. Sci.* **2024**, *14*, 244. [CrossRef]
30. Xiang, Z.; Yu, S.; Wang, X. Modeling the Hydraulic Fracturing Processes in Shale Formations Using a Meshless Method. *Water* **2024**, *16*, 1855. [CrossRef]
31. Jayakody, S.H.S.; Uzuoka, R.; Ueda, K.; Xu, J. Unsaturated slopes behavior under antecedent intermittent rainfall patterns: Centrifuge and numerical study. *Acta Geotech.* **2023**, *18*, 5773–5790. [CrossRef]
32. Duan, X.; Hou, T.; Jiang, X. Study on stability of exit slope of Chenjiapo tunnel under extreme rainstorm conditions. *Nat. Hazards* **2021**, *107*, 1387–1411. [CrossRef]
33. Guo, Y.; Du, Y.; Shan, W.; Liu, M.; Zhang, C. Numerical Analysis on the Stability of Sandstone-Covered Mudstone Cutting Slopes Considering Rainfall Infiltration. *Appl. Sci.* **2023**, *13*, 1802. [CrossRef]
34. Sun, Y.; Yang, K.; Hu, R.; Wang, G.; Lv, J. Model test and numerical simulation of slope instability process induced by rainfall. *Water* **2022**, *14*, 3997. [CrossRef]
35. Chinkulkijniwat, A.; Tirametatiparat, T.; Supotayan, C.; Yubonchit, S.; Horpibulsuk, S.; Salee, R.; Voottipruex, P. Stability characteristics of shallow landslide triggered by rainfall. *J. Mt. Sci.* **2019**, *16*, 2171–2183. [CrossRef]
36. Schilirò, L.; Marmoni, G.M.; Fiorucci, M.; Pecci, M.; Mugnozza, G.S. Preliminary insights from hydrological field monitoring for the evaluation of landslide triggering conditions over large areas. *Nat. Hazards* **2023**, *118*, 1401–1426. [CrossRef]
37. Bodman, G.B.; Colman, E.A. Moisture and Energy Conditions during Downward Entry of Water Into Soils. *Soil Sci. Soc. Am. J.* **1944**, *8*, 116–122. [CrossRef]
38. van Genuchten, M.T. A Closed-form equation for predicting the hydraulic conductivity of unsaturated Soils. *Soil Sci. Soc. Am. J.* **1980**, *44*, 892–898. [CrossRef]
39. Zolfaghari, A.R.; Heath, A.C.; Mccombie, P.F. Simple genetic algorithm search for critical non-circular failure surface in slope stability analysis. *Comput. Geotech.* **2005**, *32*, 139–152. [CrossRef]
40. Nakileza, B.R.; Nedala, S. Topographic influence on landslides characteristics and implication for risk management in upper Manafwa catchment, Mt Elgon Uganda. *Geoenviron. Disasters* **2020**, *7*, 27. [CrossRef]
41. Capitani, M.; Ribolini, A.; Bini, M. The slope aspect: A predisposing factor for landsliding? *Comptes Rendus Geosci.* **2013**, *345*, 427–438. [CrossRef]
42. Dai, F.C.; Lee, C.F. Landslide characteristics and slope instability modeling using GIS, Lantau Island, Hong Kong. *Geomorphology* **2002**, *42*, 213–228. [CrossRef]
43. Vasu, N.N.; Lee, S.R.; Pradhan, A.M.S.; Kim, Y.T.; Kang, S.H.; Lee, D.H. A new approach to temporal modelling for landslide hazard assessment using an extreme rainfall induced-landslide index. *Eng. Geol.* **2016**, *215*, 36–49. [CrossRef]
44. Ma, S.; Shao, X.; Xu, C. Landslides Triggered by the 2016 Heavy Rainfall Event in Sanming, Fujian Province: Distribution Pattern Analysis and Spatio-Temporal Susceptibility Assessment. *Remote Sens.* **2023**, *15*, 2738. [CrossRef]
45. Licata, M.; Buleo Tebar, V.; Seitone, F.; Fubelli, G. The Open Landslide Project (OLP), a New Inventory of Shallow Landslides for Susceptibility Models: The Autumn 2019 Extreme Rainfall Event in the Langhe-Monferrato Region (Northwestern Italy). *Geosciences* **2023**, *13*, 289. [CrossRef]
46. Wu, T.; Xie, X.; Wu, H.; Zeng, H.; Zhu, X. A Quantitative Analysis Method of Regional Rainfall-Induced Landslide Deformation Response Variation Based on a Time-Domain Correlation Model. *Land* **2022**, *11*, 703. [CrossRef]
47. Froude, M.J.; Petley, D.N. Global fatal landslide occurrence from 2004 to 2016. *Nat. Hazards Earth Syst. Sci.* **2018**, *18*, 2161–2181. [CrossRef]
48. Chen, P.; Mirus, B.; Lu, N.; Godt, J.W. Effect of hydraulic hysteresis on stability of infinite slopes under steady infiltration. *J. Geotech. Geoenviron. Eng.* **2017**, *143*, 04017041. [CrossRef]

49. Tan, H.; He, Z.; Yu, H.; Yang, S.; Wang, M.; Gu, X.; Xu, M. Characterization of extreme rainfall changes and response to temperature changes in Guizhou Province, China. *Sci. Rep.* **2024**, *14*, 20495. [CrossRef]
50. Yan, C.; Gong, D. Assessing framework of rainfall-induced landslide hazard considering spatiotemporal asymmetry in extreme precipitation indices under climate change. *Theor. Appl. Climatol.* **2024**, *155*, 7961–7975. [CrossRef]

Disclaimer/Publisher's Note: The statements, opinions and data contained in all publications are solely those of the individual author(s) and contributor(s) and not of MDPI and/or the editor(s). MDPI and/or the editor(s) disclaim responsibility for any injury to people or property resulting from any ideas, methods, instructions or products referred to in the content.